WILEY

ORIGINAL ARTICLE   OPEN ACCESS

Assessing the Very High Cycle Fatigue Behavior and Frequency Effect of Structural Steel Welds

Andrew England 🄳 | Yevgen Gorash 🄳 | Athanasios Toumpis 🄳

Department of Mechanical & Aerospace Engineering, University of Strathclyde, Glasgow, UK

Correspondence: Andrew England (andrew.england@strath.ac.uk)

ABSTRACT

The very high cycle fatigue behavior of S275J2+N flux-core arc welded joints was investigated using the ultrasonic fatigue testing method at a loading frequency of 20 kHz. A bespoke specimen design featuring the weld toe was employed to more suitably represent in-service welded joints than typical ultrasonic fatigue testing specimens. This revealed that fracture occurs above 10 million cycles, beyond the classically accepted fatigue limit. Additionally, comparative fatigue tests were performed at 10 Hz to investigate the frequency effect on the fatigue behavior. A 35% increase in fatigue strength was measured at 20 kHz when compared to 10 Hz, indicating that a correction must be considered in the use of ultrasonic fatigue testing data for design purposes. Fracture surfaces for both test frequencies showed similar morphologies and typical characteristics for fatigue failures of ductile metals.

1 | Introduction

The fatigue behavior of welded joints is a critical concern in structural integrity assessments of cyclically loaded structures as they are often the site of initiation and propagation of fatigue cracks [1]. The presence of local stress concentration regions, defects, inhomogeneous microstructures and residual stresses has a significant influence on the fatigue behavior of welds [2–4]. Currently, the design life of welded joints surpasses 10 million cycles, reaching the very high cycle fatigue (VHCF) domain across a range of applications, such as civil infrastructure, mineral processing equipment and offshore wind turbine monopiles [5, 6]. Performing laboratory-based VHCF testing programs using conventional fatigue testing (< 200 Hz loading frequency) is prohibitively expensive and time consuming; therefore, the ultrasonic fatigue testing (UFT) method has emerged to address this challenge [7]. UFT typically employs a 20 kHz loading frequency, which allows for 1 billion stress cycles to be achieved in 14 h [8], enabling the VHCF behavior of welds to be studied.

Despite this, there is no consensus in international standards for the course of the *S-N* curve for welded joints in the VHCF regime. For example, *S-N* curves in BS7608:2014 [9] incorporate a fatigue limit at 10 million stress cycles whereas the IIW recommendations [10] define a knee point in the *S-N* curve, but no fatigue limit.

A recently published comprehensive review on the VHCF characteristics of welds concluded that no fatigue limit exists earlier than 10^7 cycles and that the VHCF strength of welded joints is significantly reduced compared to the parent material (PM) [11]. Weldments of structural steels have garnered research interest as they are employed in applications where VHCF is experienced, for example bridges [12] and mining equipment [13]. The VHCF behavior of EH36 marine grade steel welds joined using flux-core arc welding (FCAW) was investigated by Zhao et al. [14]. Failures above 1 billion stress cycles were recorded and such, no fatigue limit was determined. He et al. [15] examined the VHCF properties of various weld zones of Q345 structural steel joined using shielded

Summary

- The very high cycle fatigue behavior of as-welded structural steel was investigated.

- Specimens failed from cracks initiating at the weld toe.

- A significant frequency effect was found using conventional fatigue testing.

metal arc welding. It was found that the fusion zone (FZ) had the lowest fatigue life due to crack initiation from welding defects [15].

Various specimen types are employed for UFT of steel welds, including cylindrical hourglass and dog-bone shaped specimens [14–22], which do not include the weld toe or root features. For these specimens, welding defects such as inclusions and gas pores are often identified as the points of crack initiation in the VHCF regime [14–21]. However, alternative specimen designs, which feature the weld toe characteristically show crack initiation at this location [23–25]. These specimens are more relevant to in-service welded structures, where fatigue cracks typically initiate from the weld toe or root as a result of the local stress concentrations [26–28]. The significance of the fatigue behaviors of these regions under cyclic loading are highlighted by fatigue assessment methods, which consider the local stresses at these points, such as the structural hot spot or notch stress approaches [10].

Structural steels exhibit a "frequency effect", i.e. an elevated fatigue strength when tested at ultrasonic frequencies [29]. The material properties of body centered cubic crystal phases, e.g. ferrite, show a sensitivity to the applied strain rate [30]. Above a transition strain rate of approx. $1–10 \, s^{-1}$ there is a change in both the dislocation mobility and fatigue crack initiation mechanism, which result in a fatigue strength increase [30]. The test frequency at which this transition strain rate occurs is assumed to be between conventional and ultrasonic frequencies [30]. The frequency effect must be considered when interpreting UFT data as in-service loads are often below the transition strain rate; for example, mining equipment typically vibrates between 12.5 and 25 Hz [13]. A significant frequency effect has been demonstrated for a range of structural steels, such as S355J0, which exhibited an approx. 55% rise in fatigue strength at 10^7 cycles when tested at 20 kHz in comparison

to 20 Hz [31]. Guennec et al. [32] introduced a frequency effect model for low, medium and high carbon steels. The model, which estimates the fatigue endurance based on the steel's yield strength, wt.% C and loading frequency, was verified by experimental data for carbon steels with a range of wt.% C. The severity of the frequency effect was shown to increase as the wt.% C decreased [32]. The influence of microstructure on the frequency effect in C15E low carbon steel was investigated by Bach et al. [33]. The annealed condition (ferritic-pearlitic microstructure) and quenched condition (bainitic microstructure) of the steel were assessed. The frequency effect was significant in the annealed condition, but insignificant in the quenched condition. Therefore, it was established that microstructure, and consequently heat treatment, has a pronounced impact on the frequency effect for steels with identical chemical composition [33], hence must be investigated for welded joints. Zhu et al. [16] performed the only research to date concerning the frequency effect of welds. 25Cr2Ni2MoV steel submerged arc welds were tested at conventional (110 Hz) and ultrasonic loading frequencies (20 kHz). The percentage increase in fatigue strength using UFT was 30% at 10^5 cycles, increasing to 75% at 10^8 cycles [16].

In the present research, the VHCF characteristics of S275J2+N flux-core arc welded joints is investigated using UFT. Comparative tests are performed using conventional fatigue testing to examine the frequency effect of low carbon steel welds, a previously unexplored research area. Both fatigue testing programs employ the same specimen design as previously proposed elsewhere [34], which features the weld toe within the gauge section, thereby allowing for the investigation of the fatigue behavior of as-welded joints.

2 | Materials and Experimental Procedures

2.1 | Materials and Welding Method

The material examined in this research was S275J2+N non-alloyed structural steel, as per EN 10025-2 [35]. All specimens were manufactured from a 12 mm thick hot rolled plate. The FCAW method was used with a 1.2 mm diameter Nippon Steel SF-1A wire, conforming with the E71T-1M classification in accordance with AWS A5.20 [36]. The nominal chemical composition and mechanical properties of the PM and as-deposited filler material are shown in Tables 1 and 2, respectively.

The 12 mm thick S275J2+N plates were milled to the required profile and reduced in thickness to 3 mm with a square edge preparation. A semi-automated rig was employed for welding to ensure the contact-tip-to-work distance (CTWD) and travel speed were consistent. A double-sided weld was used with identical parameters for each pass (Table 3), determined from an

TABLE 1 | Chemical composition of parent and as-deposited filler materials (wt%).

	C	Si	Mn	P	S	Cu
S275J2+N	0.18	0.20	0.96	0.016	0.007	0.02
E71T-1M	0.05	0.41	1.36	0.010	0.008	0.26

TABLE 2 | Mechanical properties of parent and as-deposited filler materials.

	Yield strength (MPa)	Tensile strength (MPa)	Elongation (%)	Charpy V-notch impact toughness at −20°C (J)
S275J2+N	332	480	29	137
E71T-1M	530	590	28	95

TABLE 3 | Process parameters used for FCAW.

Current (A)	Voltage (V)	Travel speed (mm/min)	CTWD (mm)	Gas flow rate (L/min)	Root gap (mm)
102–110	21.5–21.9	300	15	16	1.5
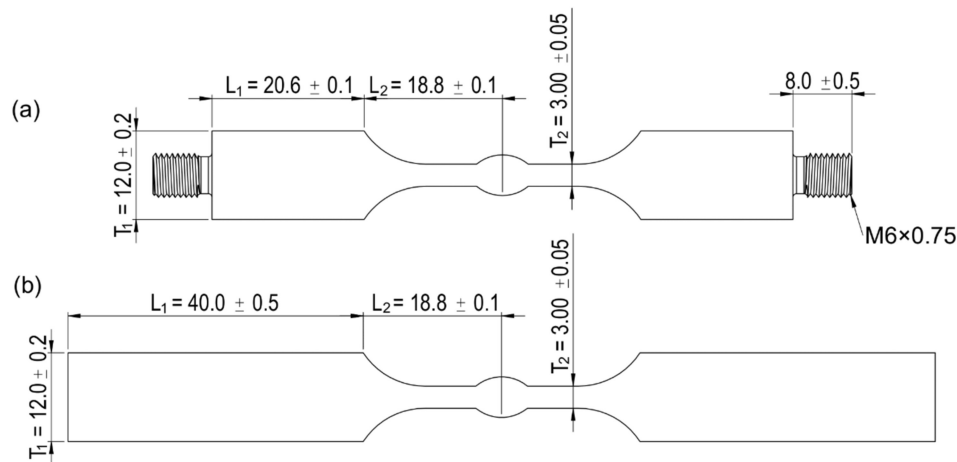
FIGURE 1 | Dimensions of fatigue specimens, all dimensions in mm (thickness 10 ± 0.1 mm): (a) UFT specimen; (b) tensile and conventional fatigue testing specimen.

extensive series of test welds. A protective shielding gas with composition 80% Ar/20% CO_2 was used.

2.2 | Microstructural Characterization and Mechanical Testing

Metallographic samples were transversely extracted from each weld to characterize the microstructure of the different weld zones and identify any possible defects. The standard metallography preparation procedure was performed on specimens, concluding with etching in a 2% Nital solution. An Olympus GX51 light optical microscope was used for microstructural characterization. A detailed Vickers microhardness map encompassing all weld zones was constructed using a Qness 60A+ automated tester, using a 0.5 kgf load and 10 s dwell time. Microhardness measurements were performed in accordance with ASTM E92-23 [37] with a grid spacing of 0.25 mm × 0.25 mm. Transverse tensile tests were completed using an Instron 8802 servohydraulic testing system with specimens identical to those used for conventional fatigue testing, as shown in Figure 1b. Two metallographic specimens and one tensile specimen were extracted from each weld, resulting in eight and four being tested, respectively.

2.3 | Fatigue Specimen Design

A novel approach was used to feature an as-welded butt joint within the gauge section of the specimen. Therefore, the cylindrical hourglass or cylindrical dog-bone shaped specimens frequently employed for UFT [19, 20] could not be used. The non-standard specimen geometry necessitated the use of linear elastic modal finite element analysis (FEA) to determine the dimensions required to resonate at 20 kHz. Analyses were performed using Abaqus FEA software, assuming

standard structural steel elastic properties (Young's modulus, E = 210 GPa, Poisson's ratio, $\nu = 0.3$, density, $\rho = 7850$ kg/m^3) [38]. A fine mesh with 67,880, eight-node linear brick elements (type C3D8) was used for both modal and harmonic analyses. The specimen dimensions T_1, T_2, and L_2 were defined as shown in Figure 1, and the dimensions of the weld bead were implemented in the FEA model. The shoulder length (L_1) was iteratively altered until a resonant frequency of 20 kHz was achieved, as shown in Figure 2a.

A specimen vibrating at its resonant frequency in the elastic deformation regime exhibits a linear proportionality of the specimen vibration amplitude and the stress amplitude [39]. The stress amplitude considered in this case was the nominal stress amplitude, i.e. neglecting the weld toe's notch effect. Harmonic analyses were performed over a range of specimen end amplitudes (10–50 μm) at a frequency of 20 kHz from which a proportionality constant $k_s = 11.40$ MPa/μm was established for programming the UFT machine. The stress distribution for a specimen end amplitude of 10 μm is shown in Figure 2b. Conventional fatigue specimens were designed with identical gauge sections to eliminate any contribution from the size effect [40] on fatigue behavior.

All testing was performed in the as-welded condition, i.e. no heat treatment or grinding of the weld toe were applied. The specimens' sides were ground longitudinally with progressively finer grit abrasive papers, up to 2400 grit. An average roughness $R_a < 0.2$ μm [41] was verified using a Mitutoyo surface roughness machine.

2.4 | Ultrasonic Fatigue Testing Details

UFT was performed at ambient temperature using a Shimadzu USF-2000A testing machine at a frequency of 20 ± 0.05 kHz
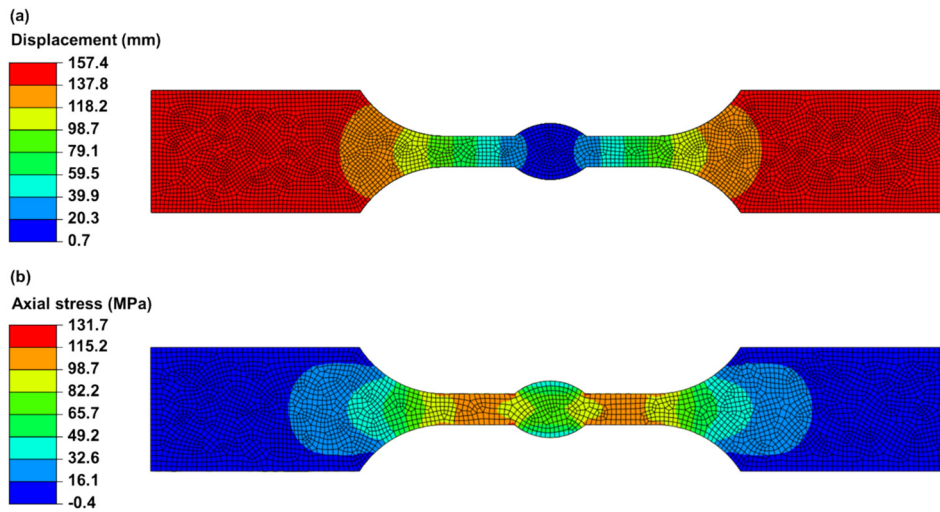
FIGURE 2 | Specimen design FEA: (a) resonant mode of vibration at 20 kHz; (b) stress amplitude for 10 μm end displacement at excitation frequency of 20 kHz. [Colour figure can be viewed at wileyonlinelibrary.com]

and a stress ratio R = −1. Calibration of the UFT system was performed pre-testing using a dummy specimen. Compressed dried air and intermittent driving were used to maintain a surface temperature less than 30°C, as required by WES 1112 [29]. A constant loading period of 110 ms was used with a variable dwell period ranging from 100 ms to 2000 ms, depending on the stress amplitude applied. An infrared thermometer was used to continuously measure the specimen surface temperature during testing, which was spray painted matte black to increase the surface emissivity [42].

Tests were terminated if either the crack detection feature of the UFT system was triggered or after 5×10^9 loading cycles had been applied. The crack detection feature continually monitors the test frequency, as a change in this indicates the presence of a significant fatigue crack [15]. The specimens in which a crack was detected were then fully fractured by monotonic loading. A Hitachi S3700-N scanning electron microscope (SEM) was used in conjunction with a digital camera with a macro lens for fracture surface analysis. Additionally, one specimen per stress amplitude was subjected to metallographic preparation to characterize the microstructure of the weld regions where fatigue crack initiation and propagation occurred. A total of 18 ultrasonic fatigue tests were performed to characterize the HCF and VHCF behavior of the welded joints.

2.5 | Conventional Fatigue Testing

An Instron 8802 servo-hydraulic fatigue testing system was used for conventional fatigue tests, in a load controlled mode. Tests were performed at ambient temperature in laboratory air. A testing frequency of 10 Hz was employed for tensile-tensile (R = 0.1) cyclic loading and specimen cooling was not required due to the lower test frequency. Tests were terminated when specimens completely fractured, or after 2.5×10^6 cycles had been applied. Fracture surface analysis was performed in the same methods as with UFT and 13 specimens were tested in total.

3 | Results

3.1 | Microstructural Characterization

A representative macrograph of the welded joint's cross-section is displayed in Figure 3a. The parent material (Figure 3b) consisted of a high volume fraction of equiaxed ferrite in addition to smaller pearlite grains. Ferrite-pearlite banding can be observed, a common occurrence in hot rolled non-alloyed steels [43, 44]. The fine-grained heat affected zone (HAZ) (Figure 3c), exhibited smaller ferrite grain sizes than the PM. Additionally, the prior ferrite colonies have decomposed into much finer pearlite and ferrite grains upon cooling. The coarse-grained HAZ (Figure 3d) consisted of both acicular ferrite and bainite as a result of the high cooling rate experienced in this region. The FZ presented a predominately fine-grained ferrite microstructure (Figure 3e), due to the low carbon content of the filler wire used (0.05 wt% C). No identifiable defects, e.g. porosity or incomplete fusion, were observed.

3.2 | Hardness Distribution

As shown in Figure 4, the sample's hardness demonstrated a heterogeneous distribution across the weld, a consequence of the varied grain sizes and microstructures observed. The region with the lowest hardness was the PM due to the relatively large ferrite grain size. The HAZ exhibited increased hardness compared to the PM, due to the identified grain refinement (Figure 3c). The peak hardness was recorded in the coarse-grained HAZ, attributed to the microstructure of acicular ferrite and bainite. The hardness distribution across the FZ is relatively constant at approx. 200 HV, consistent with previous studies on low carbon steel welds [14, 15].

3.3 | Tensile Testing

All tensile test samples failed in a ductile mode in the PM, verifying the high static strength of the weld. Transverse tensile
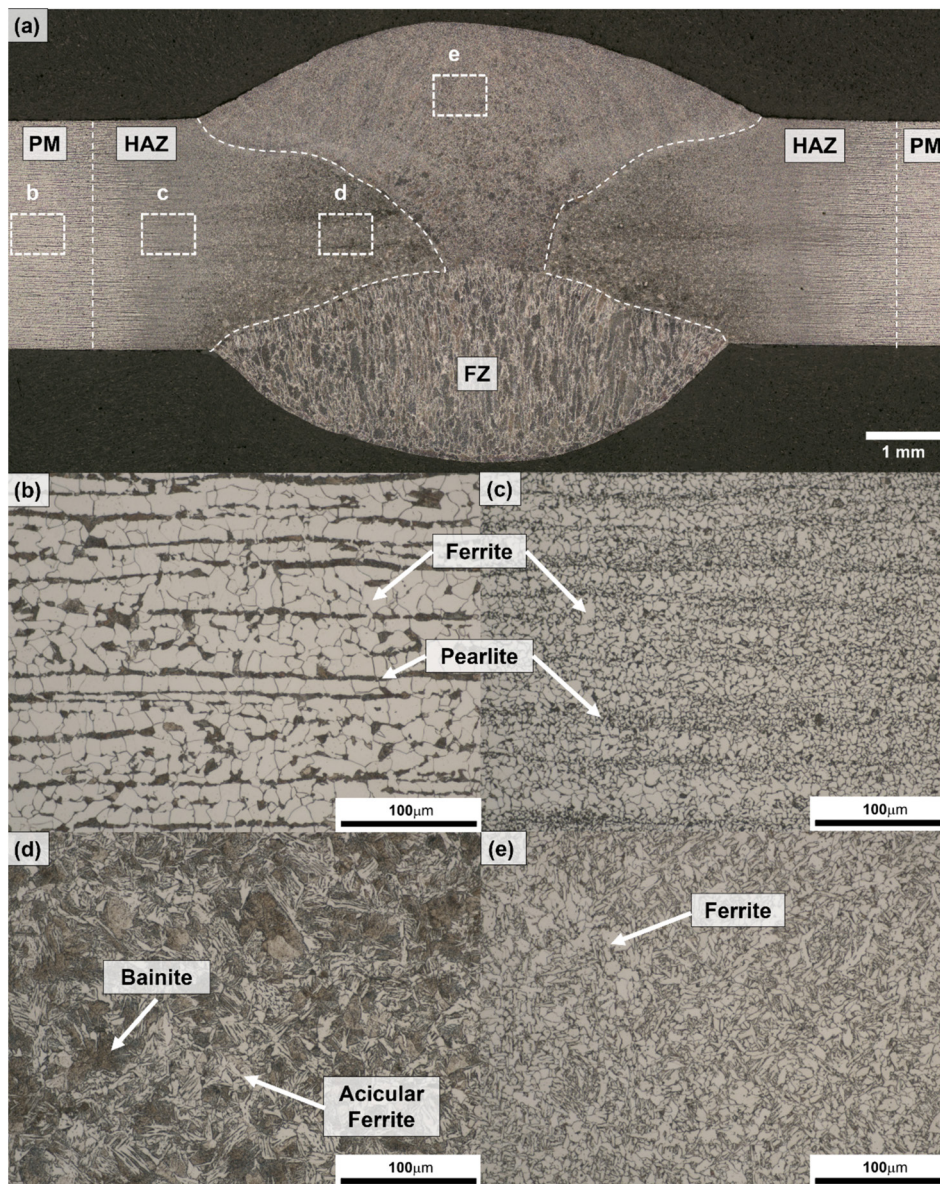
FIGURE 3 | Microstructure of S275J2+N weld: (a) macrograph showing weld regions [×50, etched]; (b) PM [×500, etched]; (c) fine-grained HAZ [×500, etched]; (d) coarse-grained HAZ [×500, etched]; (e) FZ [×500, etched]. [Colour figure can be viewed at wileyonlinelibrary.com]
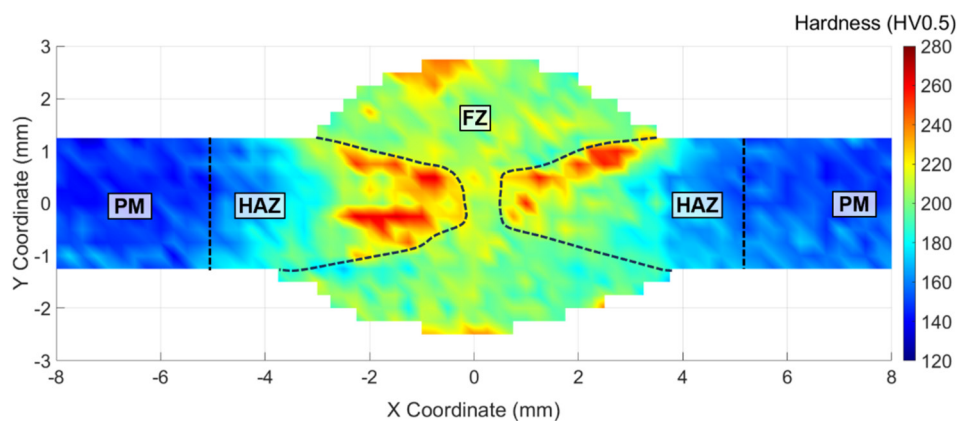

FIGURE 4 | Vickers microhardness map of welded joint. [Colour figure can be viewed at wileyonlinelibrary.com]

tests are extensively used in industry to evaluate the strength of welds, with failure in the PM qualifying the weld [45]. The average yield strength and tensile strength recorded were 320 MPa and 507 MPa, respectively, which both comply with the standard EN 10025-2 [35] for S275J2+N.

3.4 | Ultrasonic Fatigue Testing

3.4.1 | *S-N* Curves

Figure 5 displays the UFT results and associated mean and design *S-N* curves. The maximum applied stress varied from 70% to 35% of the yield strength of the PM, and failures were recorded between 2.21×10^5 to 8.25×10^8 cycles. Generally, the number of cycles to failure increased as the applied stress decreased. The bilinear *S-N* curve was constructed by splitting the data into high cycle fatigue (HCF) and VHCF data sets, using a threshold of 10^7 cycles. Each of these regions were then fit to the standard form of the *S-N* curve using least squares regression [10]. The HCF and VHCF *S-N* curves were extended to an intercept point at approx. 9.74×10^6 cycles. Design *S-N* curves were also derived for a 95% survival probability [10], with the parameters given in Table 4.

The mean *S-N* curve shows a continuous decrease in both HCF and VHCF regimes, with a shallower slope in the VHCF regime. The values of the *S-N* curve's slope in the HCF regime (m = 6.9) and VHCF regime (m′ = 51) are similar to those proposed by Baumgartner et al. [46] at m = 5 and m′ = 45. The existence of a knee point at the transition from HCF to VHCF is also observed by other researchers [14, 24] and is included in the IIW recommendations [10]. No distinct fatigue limit was observed for the welded joint, with fatigue failures occurring at a maximum of 8.25×10^8 cycles at a stress amplitude of 114 MPa. This further adds to the general trend observed that a constant amplitude fatigue limit does not occur at less than 10^7 cycles, as conventionally assumed [11]. Two runout specimens, which did not fail after 5×10^9 cycles were recorded for stress amplitudes of 128 MPa and 114 MPa. The results show scatter with variation in fatigue life at the same stress

amplitude, a result aligning with previous research for both non-welded and welded steels [14, 15, 47, 48].

3.4.2 | Fatigue Crack Path Analysis

All failed specimens exhibited fatigue cracks initiating from the weld toe, with a representative example shown in Figure 6. A single significant fatigue crack was typically observed on the specimen surface after UFT was terminated (Figure 6a). It was identified that there was an equal probability of the crack initiating at either the first or second weld pass. Only one specimen exhibited fatigue cracking from multiple weld toes ($\sigma_a = 192$ MPa, $N_f = 1.39 \times 10^6$). No fatigue cracks were observed in the PM region for any tests.

It is generally observed that fatigue cracks propagate perpendicular to the loading direction in a homogenous material [49]; however, the fatigue cracks observed in the welded specimens were generally at an angle slightly inclined to perpendicular (approx. 10^0–15^0). Previous research has indicated that this behavior is characteristic of crack propagation in the HAZ [28]. Additionally, the direction of crack propagation was generally towards the coarse-grained HAZ (Figure 6b). This behavior can be explained by the findings of Nishikawa et al. [50], who revealed that the coarse-grained HAZ had a greater fatigue crack growth rate compared to the fine-grained HAZ

TABLE 4 | *S-N* curve parameters for ultrasonic and mean stress corrected conventional fatigue testing results.

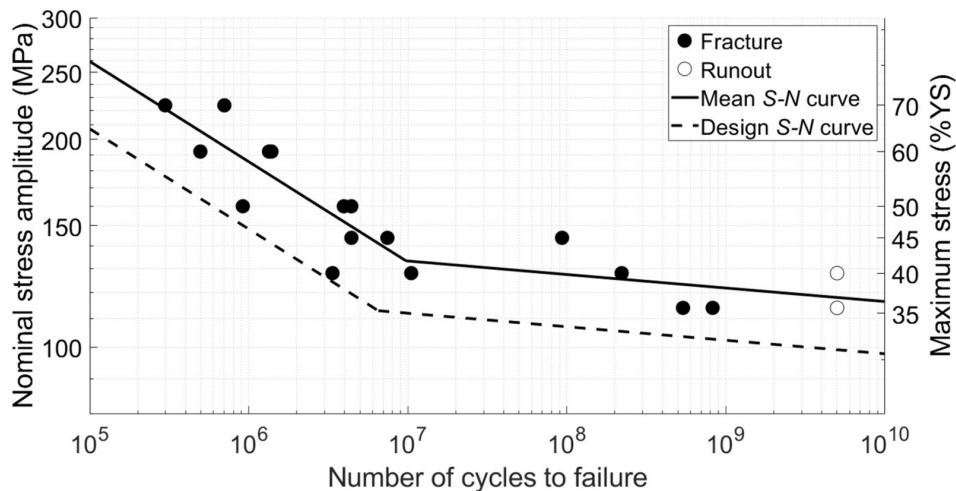| *S-N* curve	Regime	C	m
20 kHz mean	HCF	4.16×10^{21}	6.89
	VHCF	2.91×10^{115}	51.0
20 kHz design	HCF	8.86×10^{20}	6.89
	VHCF	4.00×10^{111}	51.0
10 Hz mean	HCF	1.55×10^{21}	7.07
10 Hz design	HCF	1.01×10^{21}	7.07

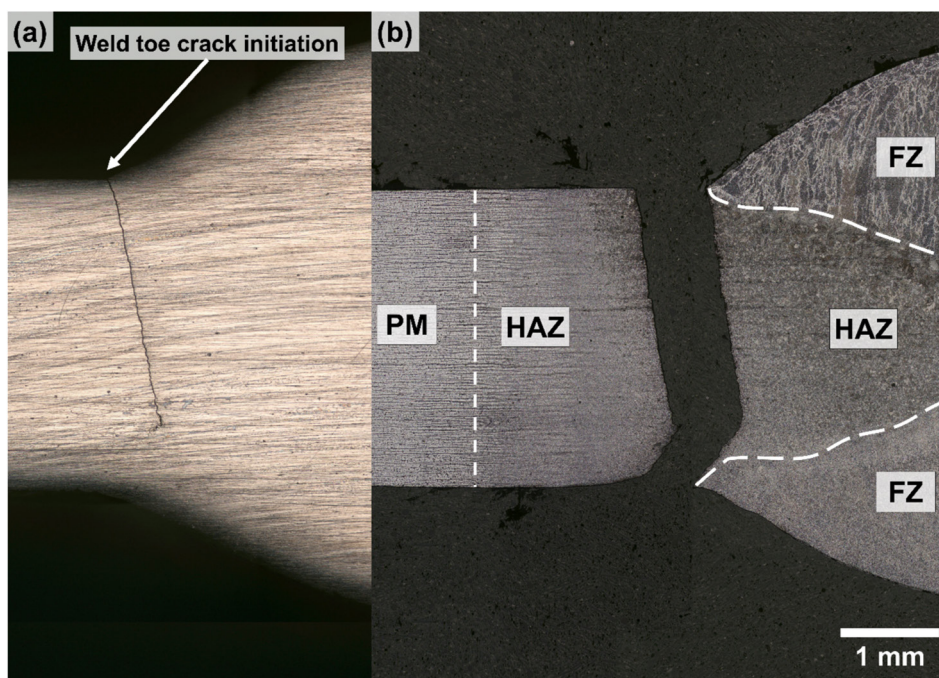**FIGURE 5** | UFT results and *S-N* curves.

FIGURE 6 | Representative fatigue fracture location ($\sigma_a = 160\,\text{MPa}$, $N_f = 9.17 \times 10^5$ cycles): (a) fatigue crack after termination of UFT [×50]; (b) complete fracture after monotonic loading [×50, etched]. [Colour figure can be viewed at wileyonlinelibrary.com]
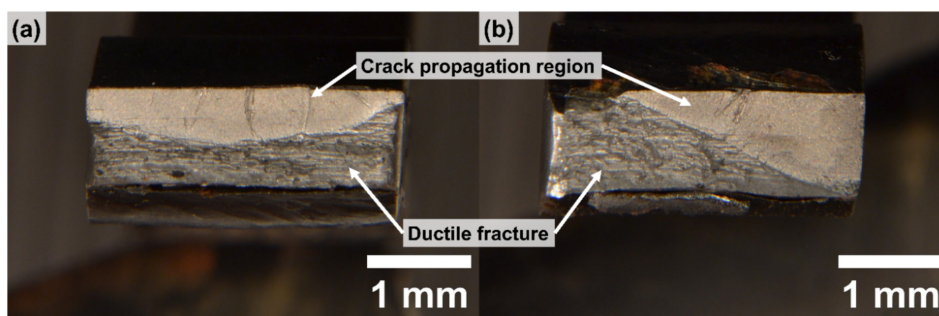

FIGURE 7 | Fracture surfaces of UFT specimens: (a) HCF failure ($\sigma_a = 192\,\text{MPa}$, $N_f = 1.36 \times 10^6$ cycles); (b) VHCF failure ($\sigma_a = 114\,\text{MPa}$, $N_f = 5.37 \times 10^8$ cycles). [Colour figure can be viewed at wileyonlinelibrary.com]

for a low carbon steel weld. A further publication from the same research group [51] found that the coarse-grained HAZ demonstrated a lower VHCF strength than the fine-grained region. Therefore, it was determined that the coarse-grained HAZ presented the path of least resistance for fatigue crack propagation in the tested welds.

3.4.3 | Fractography

Fracture surface analysis was employed for characterization of the fatigue crack initiation sites and propagation surfaces of the failed specimens. Two different but recurrent fracture surface morphologies were observed for failed UFT specimens, for which representative examples are displayed in Figure 7. Specimens tested at a greater stress amplitude consistently exhibited semi-elliptical cracks that spanned the full width of the specimen (Figure 7a). In contrast, specimens tested at lower applied stresses, which failed in the VHCF regime, demonstrated fatigue cracks through the entire specimen thickness at one edge

(Figure 7b). The ductile failure region was identified by dimples and microvoids, and was a result of the monotonic loading used to separate the specimens.

The displacement control method employed in UFT requires a linear relationship between the vibration amplitude and stress amplitude [39]. This relationship relies on the assumption of elastic material behavior; consequently, it must be verified through fractography that excessive bulk plastic deformation has not occurred during fatigue loading, as described by Swacha and Lipski [39]. The specimens' crack propagation region revealed no indications of significant plastic deformation, e.g. necking or dimples, and therefore it was verified that the assumption of a direct proportionality between vibration amplitude and stress amplitude was valid.

It was revealed using SEM that all cracks initiated from the specimen surface at the weld toe, as shown in Figure 8. The crack growth direction was then found to be radial, outwards from the initiation point, as demonstrated by river marks on the
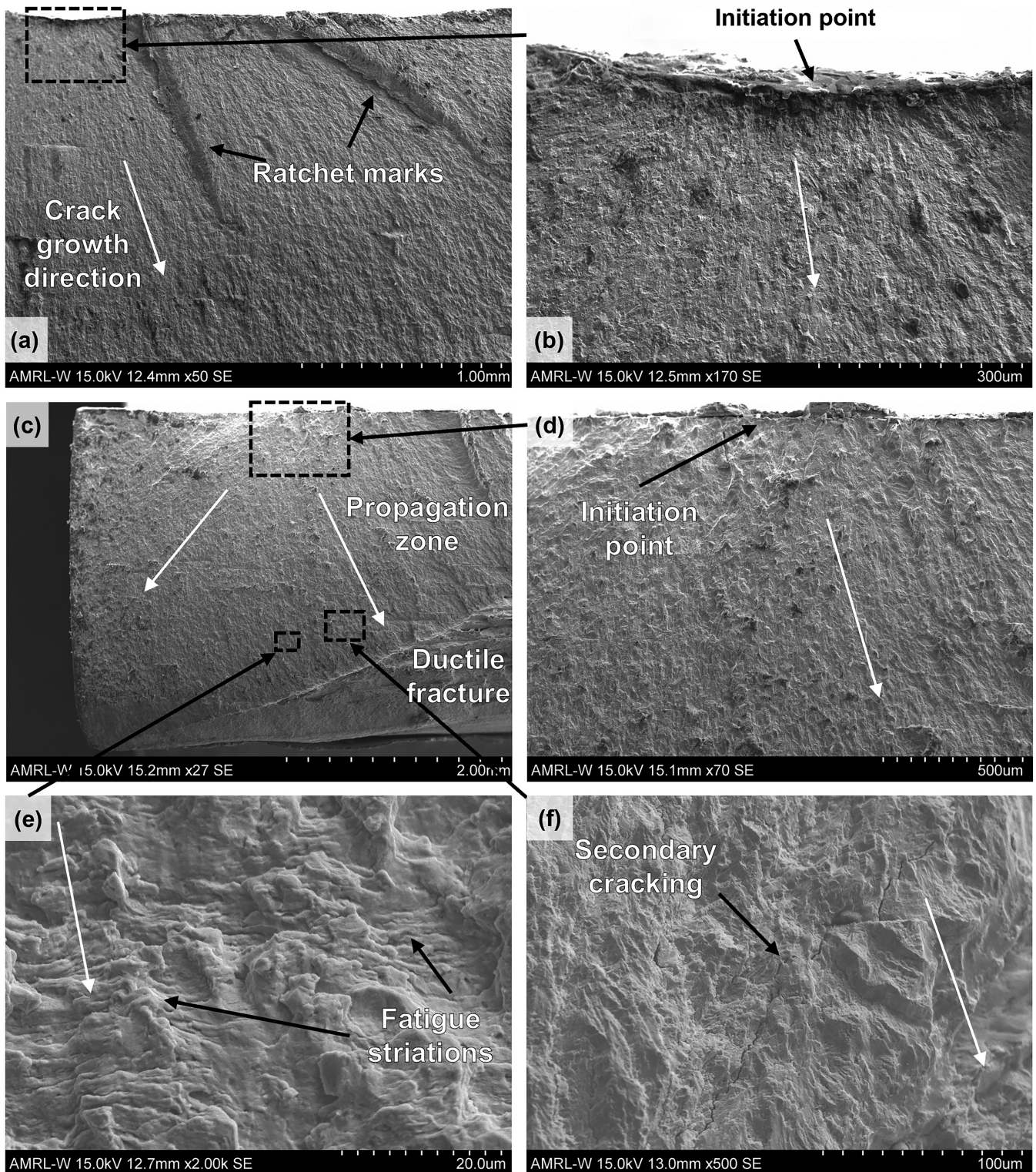
FIGURE 8 | SEM micrographs of fracture surfaces of UFT specimens (white arrows indicate direction of crack propagation): (a, b) HCF failure ($\sigma_a = 160$ MPa, $N_f = 3.96 \times 10^6$ cycles); (c, d, e, f) VHCF failure ($\sigma_a = 114$ MPa, $N_f = 5.37 \times 10^8$ cycles).

propagation surface. The presence of river marks also indicated a transgranular crack growth mechanism [52]. HCF fracture surfaces typically displayed ratchet marks, indicating multiple crack origin sites (Figure 8a). This observation is typical of fatigue failures resulting from relatively high applied stresses [53]. Figure 8b displays a crack initiation point from a minor undercut, illustrating the importance of weld quality for structural

integrity of joints. The fracture surfaces of VHCF failures typically only displayed single sites of crack initiation, as shown in Figure 8c,d. Fatigue striations orientated approximately perpendicular to the crack growth direction were observed at various locations on the fracture surfaces under high magnification, as shown in Figure 8e. The relative smoothness of these compared to typical, well defined striations, is a result of the low R ratio

and applied stress [54]. Secondary cracking was infrequently identified on fracture surfaces; an example of this is given in Figure 8f. Overall, fracture surfaces displayed typical features of ductile fatigue failures.

3.5 | Conventional Fatigue Testing

3.5.1 | *S-N* Curves

The conventional fatigue testing results and associated *S-N* curves are shown in Figure 9. Failed specimens were fitted to a single slope *S-N* curve, as the conventional test method only allowed the behavior in the HCF regime to be investigated. Tests with maximum stresses equivalent to 90% to 70% of the yield strength of the PM resulted in failures between 2.31×10^5 and 1.54×10^6 cycles. Crack initiation solely occurred at the weld toe, identical to observations from failed UFT specimens. Relatively low variation was observed in tests at 90% and 80% of the yield strength, with a similar number of cycles to failure recorded across different specimens tested at the same stress amplitude. In contrast, the results at the lowest stress amplitude displayed a greater scatter, with two fractured specimens and three runout specimens recorded. The gradient of the conventional fatigue testing *S-N* curve is similar to that found using UFT at m = 7.1. A fatigue limit at approx. 2×10^6 was noted for structural steel butt welds by Schaumann and Steppeler [55], which is similar to this research.

3.5.2 | Fractography

Typical fracture surfaces from conventional fatigue specimens are presented in Figure 10. The surface morphologies were very similar to what was observed for UFT specimens; crack initiation occurred at the weld toe and was followed by a relatively featureless crack propagation region. One difference between specimens tested with the two methods lies in the transition from the propagation surface to the ductile fast fracture one. The termination of cyclic loading in UFT due to the frequency change followed by monotonic fracture results in a distinct boundary between the two regions on the fracture surface (Figure 7). As the conventional specimens are cyclically loaded until complete fracture, the boundary is less apparent, although the fast fracture region can still be clearly identified. The fatigue crack path of conventional test specimens showed similar characteristics as the UFT specimens.

4 | Discussion

4.1 | Assessment of Frequency Effect

The ultrasonic and conventional fatigue tests were carried out at R = −1 and R = 0.1, respectively, therefore the mean stress effect had to be considered to compare results. Mean stress correction was performed using the FKM guidelines [56] to convert the stress amplitude at R = 0.1 to an equivalent damage stress
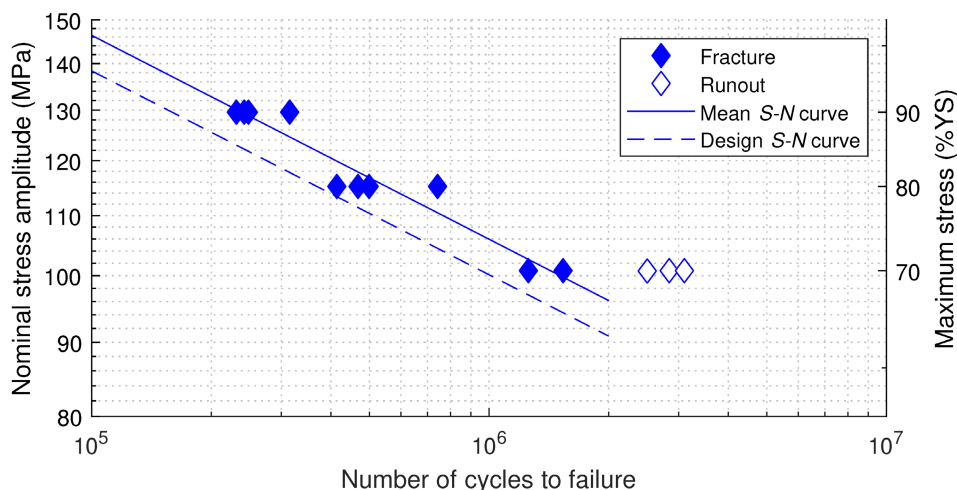

FIGURE 9 | Conventional fatigue testing results and *S-N* curves. [Colour figure can be viewed at wileyonlinelibrary.com]
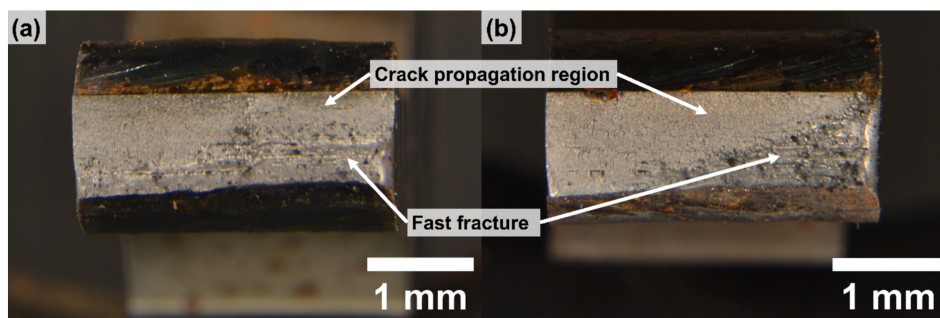

FIGURE 10 | Fracture surfaces of conventional fatigue testing specimens: (a) high stress amplitude specimen ($\sigma_a = 130$ MPa, $N_f = 2.42 \times 10^5$ cycles); (b) low stress amplitude specimen ($\sigma_a = 101$ MPa, $N_f = 1.26 \times 10^6$ cycles). [Colour figure can be viewed at wileyonlinelibrary.com]

amplitude at R = −1. The mean stress correction depends on the assumed residual stress state in the weld [56]. Previous research has indicated that extracting specimens from welded joints significantly reduces the residual stress [57, 58]. He et al. [59] measured residual stresses of very low magnitude (11.1 MPa in the transverse direction) in arc welded weathering steel UFT specimens. Thus, the residual stresses in the UFT and conventional fatigue specimens were assumed to be similarly low in magnitude due to their small size. A mean stress sensitivity of 0.3 was used and, as a result, the conventional fatigue testing stress amplitudes were divided by a mean stress factor of 0.754. It was also verified through FEA that loading at 10 Hz and 20 kHz resulted in the same stress concentration factor at the weld toe. The ultrasonic and conventional fatigue testing results, with corrected stress amplitude, are plotted in Figure 11 and coefficients of all S-N curves are given in Table 4. The UFT design S-N curve lies completely above the conventional fatigue fractures and S-N curves. Therefore, it is evident that using UFT test data would lead to un-conservative design of cyclically loaded welded structures.

The frequency effect was quantified using the frequency coefficient, F, in line with Zhu et al. [16]. The frequency coefficient represents the factor increase in the fatigue strength at 20 kHz compared to 10 Hz. The values of the mean S-N curve were used for this purpose and, as the slope is almost equivalent over the HCF region, a constant value of F = 1.35 was established. This value is intrinsically related to the mean stress sensitivity correction factor used, but there is a significant increase in fatigue strength using ultrasonic loading compared to conventional. The different failure criteria employed for ultrasonic and conventional methods were regarded to have a negligible influence on the fatigue life, due to the fracture surfaces from each test method showing similar morphologies. For submerged arc welded joints of 25Cr2Ni2MoV alloy steel, Zhu et al. [16] measured a frequency coefficient, which increased from 1.30 at 10^5 cycles, to 1.75 at 10^8 cycles. The presently studied S275J2+N FCAW joints exhibit a similar frequency effect in the HCF regime, however Zhu et al. [16] observed fractures in the PM in this regime, which limits comparison of results.

The measured frequency effect of the welded joint was compared with the model introduced by Guennec et al. [32], which estimates a fatigue endurance value. The fatigue endurance is valid for un-notched PM; therefore, this value could not be used for comparison. Instead, a predicted frequency coefficient, F_G, was calculated using the expected increase in fatigue endurance for tests performed at 10 Hz and 20 kHz. For S275J2+N with 0.18 wt.% C, this was determined to be $F_G = 1.61$. Comparing this to the measured frequency sensitivity (F = 1.35), it is evident the severity of the frequency effect is reduced for low carbon steel welds when compared to that of the PM.

It has been previously identified that one cause of the frequency effect is the transition in the fatigue crack initiation mechanism, from transgranular at conventional loading frequency to intergranular at ultrasonic loading frequency [30]. Yet, in the fatigue assessment of welded structures, a common assumption is the crack initiation period is negligible compared to the propagation period as a result of weld toe flaws [60]. The yield strength of low carbon steels has been shown to be dependent to the applied strain rate, which would consequently cause the observed frequency effect in the studied welds [61].

Assessing the fatigue behavior of the welded joint in the VHCF regime using conventional fatigue testing would enable further insight into the frequency effect, however this would be prohibitively time consuming. Employing an intermediate loading frequency, e.g. 100 Hz–1000 Hz, should be a focus of future research in this area.

4.2 | Notch Stress Assessment

The fatigue strength of the welds at each loading frequency was assessed with the notch stress method [62]. The S-N curves for this approach are based on a range of experimental data for weld toe or root initiated failure, therefore allowing for the fatigue testing results from the current investigation to be compared. A reference radius $r_{ref} = 0.3$ mm was used following the recommendations proposed by Baumgartner et al. [46] for welds of low
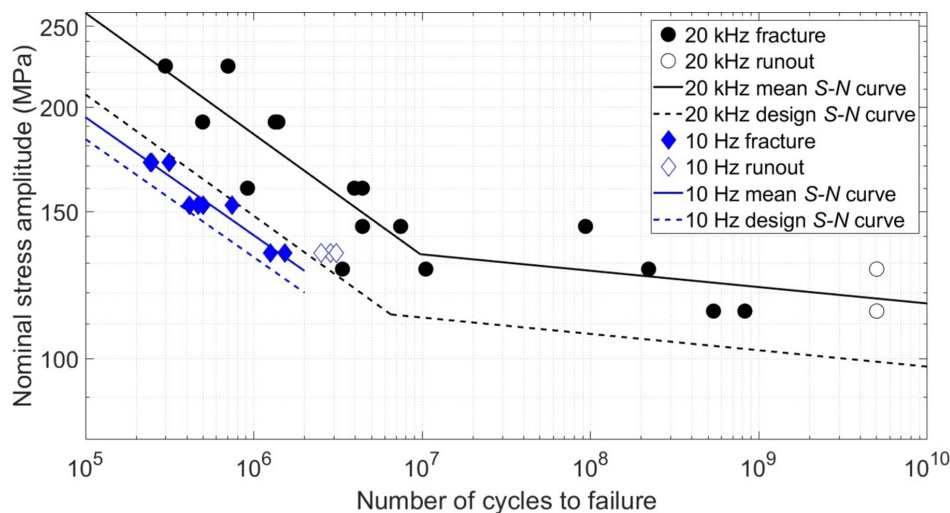

FIGURE 11 | Comparison of ultrasonic and mean stress corrected conventional fatigue testing results. [Colour figure can be viewed at wileyonlinelibrary.com]
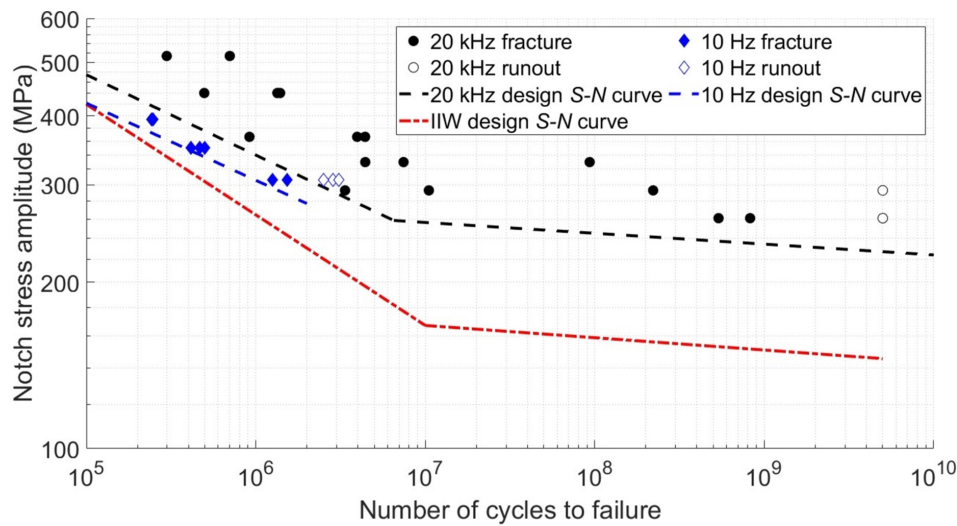
FIGURE 12 | Fatigue testing results evaluated with notch stress approach. [Colour figure can be viewed at wileyonlinelibrary.com]

thickness (< 10 mm). The maximum local principal stress was determined using a linear elastic FEA model with the meshing specification outlined by Bruder et al. [63]. From this, a stress concentration factor $K_t = 2.290$ was found. The weld opening angle was measured from metallography specimens to be approx. 145°, thus the FAT 300 design curve was used [46]. This design curve is derived for R = 0.5, therefore the FAT value was transformed to a damage equivalent stress at R = −1 using the FKM guidelines [56]. Additionally, slopes of m = 5 and m′ = 45 were considered for the HCF and VHCF regimes, respectively, following Baumgartner et al. [46]. The evaluation of the fatigue results following conversion to notch stress is shown in Figure 12.

All fatigue failures lie above the IIW design curve in both HCF and VHCF regimes. The 10 Hz design curve converges with the IIW design curve at around 10^5 cycles, although no fatigue failures were recorded at this lifetime in experiments. The design curves for the experimental data sets have a decreased slope when compared to the IIW design curve and, accordingly, they increasing diverge as the number of cycles increases. Consequently, the IIW design curve is conservative compared to the experimental data in the VHCF regime.

5 | Conclusions

In this research, the VHCF behavior and frequency effect of FCAW joints of S275J2+N structural steel were investigated using the ultrasonic and conventional fatigue testing methods. A novel specimen design enabling the assessment of the VHCF behavior of as-welded joints was successfully employed using UFT. From this, it was demonstrated that the welded joints exhibited multiple fatigue failures in the VHCF regime, in contrast to the conventionally assumed fatigue limits. Fatigue failure occurred at a maximum of 8.25×10^8 cycles and no fatigue limit was observed. A bilinear S-N curve was fitted to the UFT data and displayed a reduced slope in the VHCF regime (m′ = 51) compared to the HCF regime (m = 6.9), in agreement with previous research and the IIW recommendations.

It was confirmed that the cyclic loading frequency has an influence on the fatigue behavior of structural steel welds. The fatigue strength was increased at ultrasonic loading frequency when compared to conventional frequency by a factor of 1.35. Consequently, the use of UFT data without any consideration of the frequency effect will lead to un-conservative design of welded steel structures. Additionally, the fatigue behavior of the welds was assessed using the notch stress approach and showed superior fatigue strength compared to the IIW recommendations within the VHCF regime.

Author Contributions

Andrew England: conceptualization, methodology, investigation, formal analysis, writing – original draft, visualization. **Yevgen Gorash:** conceptualization, methodology, writing – review and editing, supervision. **Athanasios Toumpis:** conceptualization, methodology, writing – review and editing, supervision.

Conflicts of Interest

The authors declare no conflicts of interest.

Data Availability Statement

The data that support the findings of this study are available from the corresponding author upon reasonable request.

References

1. M. Braun and X. Wang, "A Review of Fatigue Test Data on Weld Toe Grinding and Weld Profiling," *International Journal of Fatigue* 145 (2021): 106073.

2. D. Q. Q. Wang, D. D. Yao, Q. Wang, Z. B. Gao, Z. F. Zhang, and X. W. Li, "Evaluating the Fatigue Property of S355J2W Steel Butt-Welded

Joint: Multiple Notch Effects," *International Journal of Fatigue* 167 (2023): 107362.

3. S. Tsutsumi, R. Fincato, P. Luo, et al., "Effects of Weld Geometry and HAZ Property on low-Cycle Fatigue Behavior of Welded Joint," *International Journal of Fatigue* 156 (2022): 106683.

4. D. Rozumek, J. Lewandowski, G. Lesiuk, Z. Marciniak, J. A. Correia, and W. Macek, "The Energy Approach to Fatigue Crack Growth of S355 Steel Welded Specimens Subjected to Bending," *Theoretical and Applied Fracture Mechanics* 121 (2022): 103470.

5. G. Alencar, A. de Jesus, J. G. S. da Silva, and R. Calçada, "Fatigue Cracking of Welded Railway Bridges: A Review," *Engineering Failure Analysis* 104 (2019): 154–176.

6. A. Mehmanparast, A. Chahardehi, F. Brennan, and M. Manzocchi, "Re-Evaluation of Fatigue Design Curves for Offshore Wind Monopile Foundations Using Thick as-Welded Test Specimens," *Engineering Failure Analysis* 158 (2024): 158.

7. M. Fitzka, B. M. Schönbauer, R. K. Rhein, et al., "Usability of Ultrasonic Frequency Testing for Rapid Generation of High and Very High Cycle Fatigue Data," *Materials* 14 (2021): 14.

8. H. Kuhn and D. Medlin, "Ultrasonic Fatigue Testing," in *Mechanical Testing and Evaluation*, vol. 8 (Materials Park, USA: ASM International, 2000), 717–729.

9. BS 7608:2014, *Guide to Fatigue Design and Assessment of Steel Products* (London, UK: British Standards Institution, 2014).

10. A. F. Hobbacher, *Recommendations for Fatigue Design of Welded Joints and Components* (Cham: Springer International Publishing, 2016).

11. A. England, A. Toumpis, and Y. Gorash, "Very High Cycle Fatigue of Welds: A Review," *Metals (Basel)* 13 (2023): 1860.

12. C. He, Y. Liu, D. Fang, and Q. Wang, "Very High Cycle Fatigue Behavior of Bridge Steel Welded Joint," *Theoretical and Applied Mechanics Letters* 2 (2012): 31010.

13. P. R. Fry, "High Cycle Fatigue of Welded Structures: Design Guidelines Validated by Case Studies," *Engineering Failure Analysis* 46 (2014): 179–187.

14. X. Zhao, W. Dongpo, C. Deng, Y. Liu, and S. Zongxian, "The Fatigue Behaviors of Butt Welds Ground Flush in the Super-Long Life Regime," *International Journal of Fatigue* 36 (2012): 1–8.

15. C. He, C. Huang, Y. Liu, and Q. Wang, "Fatigue Damage Evaluation of low-Alloy Steel Welded Joints in Fusion Zone and Heat Affected Zone Based on Frequency Response Changes in Gigacycle Fatigue," *International Journal of Fatigue* 61 (2014): 297–303.

16. M. L. Zhu, L. L. Liu, and F. Z. Xuan, "Effect of Frequency on Very High Cycle Fatigue Behavior of a low Strength Cr-Ni-Mo-V Steel Welded Joint," *International Journal of Fatigue* 77 (2015): 166–173.

17. M. L. Zhu and F. Z. Xuan, "Failure Mechanisms and Fatigue Strength Assessment of a low Strength Cr–Ni–Mo–V Steel Welded Joint: Coupled Frequency and Size Effects," *Mechanics of Materials* 100 (2016): 198–208.

18. P. Wang, W. Wang, M. Zhang, Q. Zhou, and Z. Gao, "Effects of Specimen Size and Welded Joints on the Very High Cycle Fatigue Properties of Compressor Blade Steel KMN-I," *Coatings* 11 (2021): 1244.

19. M. Zhang, H. Zhang, M. Li, L. Liu, and P. Wang, "Fatigue Behavior and Mechanism of dog-Bone-Shaped Specimens of FV520B-I in a Very High Cycle Regime," *Fatigue and Fracture of Engineering Materials and Structures* 45 (2022): 3658–3676.

20. M. Zhang, W. Wang, P. Wang, Y. Liu, and J. Li, "Fatigue Behavior and Mechanism of FV520B-I Welding Seams in a Very High Cycle Regime," *International Journal of Fatigue* 87 (2016): 22–37.

21. Z. Xiong, E. Peng, L. Zeng, and Q. Xu, "Giga-Cycle Fatigue Behavior of the Nuclear Structure of 316L Weldments," *Frontiers in Energy Research* 9 (2021): 9.

22. Z. Xiong, D. Wei, H. Wang, H. J. Shi, and X. Ma, "Fatigue Behavior of 316 L Stainless Steel Weldment up to Very-High-Cycle Fatigue Regime," *Materials Research Express* 6 (2019): 076514.

23. Z. Gao, D. Wang, B. Gong, C. Deng, S. Wu, and H. Zhang, "VHCF Behavior of Welded Joints With HFMI Treatment Under Moisture Conditions," *Welding Journal* 101 (2022): 27–42.

24. Y. Liu, C. He, C. Huang, M. K. Khan, and Q. Wang, "Very Long Life Fatigue Behaviors of 16Mn Steel and Welded Joint," *Structural Engineering and Mechanics* 52 (2014): 889–901.

25. D. Yin, D. Wang, H. Jing, and L. Huo, "The Effects of Ultrasonic Peening Treatment on the Ultra-Long Life Fatigue Behavior of Welded Joints," *Materials and Design* 31 (2010): 3299–3307.

26. D. H. Phillips, *Welding Engineering: An Introduction* (Chichester: Wiley, 2016).

27. P. Moore and G. Booth, *The Welding Engineer's Guide to Fracture and Fatigue* (Amsterdam, Netherlands: Elsevier, 2015).

28. M. Benedetti, V. Fontanari, and C. Santus, "Crack Growth Resistance of MAG Butt-Welded Joints of S355JR Construction Steel," *Engineering Fracture Mechanics* 108 (2013): 305–315.

29. WES 1112, "Method for Ultrasonic Fatigue Testing in Metallic Material," (2022).

30. B. Guennec, A. Ueno, T. Sakai, M. Takanashi, Y. Itabashi, and M. Ota, "Dislocation-Based Interpretation on the Effect of the Loading Frequency on the Fatigue Properties of JIS S15C low Carbon Steel," *International Journal of Fatigue* 70 (2015): 328–341.

31. J. Klusák, V. Horník, G. Lesiuk, and S. Seitl, "Comparison of High- and low-Frequency Fatigue Properties of Structural Steels S355J0 and S355J2," *Fatigue and Fracture of Engineering Materials and Structures* 44 (2021): 3202–3213.

32. B. Guennec, T. Kinoshita, N. Horikawa, N. Oguma, and T. Sakai, "Loading Frequency Effect on the Fatigue Endurance of Structural Carbon Steels: Estimation Based on Dislocation Motion Theory and Experimental Verification of the Model," *International Journal of Fatigue* 172 (2023): 107634.

33. J. Bach, M. Göken, and H.-W. Höppel, "Fatigue of low Alloyed Carbon Steels in the HCF/VHCF-Regimes," in *Fatigue of Materials at Very High Numbers of Loading Cycles*, ed. H. J. Chris (Wiesbaden, Germany: Springer Spektrum, 2018), 1–23.

34. A. England, A. Toumpis, and Y. Gorash, "Specimen Design for Gigacycle Fatigue Testing of Structural Steel Welded Joints," *Procedia Structural Integrity* 57 (2023): 494–501.

35. BS EN 10025–2:2004, "Hot Rolled Products of Structural Steels. Technical Delivery Conditions for Non-Alloy Structural Steels," (2019).

36. AWS A5.20/A5.20M:2005, "Specification for Carbon Steel Electrodes for Flux Cored Arc Welding," (2005).

37. ASTM E92-23, "Standard Test Methods for Vickers Hardness and Knoop Hardness of Metallic Materials," (2023).

38. BS EN 1993-1-1:2022, "Eurocode 3 - Design of Steel Structures - General Rules and Rules for Buildings," (2022).

39. P. Swacha and A. Lipski, "Cracking of S355J2+N Steel in the High-Cycle and Very-High-Cycle Fatigue Regimes," *International Journal of Fatigue* 168 (2023): 107388.

40. Y. Furuya, "Notable Size Effects on Very High Cycle Fatigue Properties of High-Strength Steel," *Materials Science and Engineering A* 528 (2011): 5234–5240.

41. ASTM E466-21, "Standard Practice for Conducting Force Controlled Constant Amplitude Axial Fatigue Tests of Metallic Materials," (2021).

42. Y. Gorash, T. Comlekci, G. Styger, J. Kelly, F. Brownlie, and L. Milne, "Ultrasonic Fatigue Testing of Structural Steel S275JR+AR With

Insights Into Corrosion, Mean Stress and Frequency Effects," *Materials* 16 (2023): 1799.

43. S. E. Offerman, N. H. Van Dijk, M. T. Rekveldt, J. Sietsma, and S. Van der Zwaag, "Ferrite/Pearlite Band Formation in hot Rolled Medium Carbon Steel," *Materials Science and Technology* 18 (2002): 297–303.

44. J. Lewandowski and D. Rozumek, "Fatigue Crack Growth in Welded S355 Samples Subjected to Bending Loading," *Metals (Basel)* 11 (2021): 1394.

45. Z. L. Zhang, M. Hauge, C. Thaulow, and J. Ødegård, "A Notched Cross Weld Tensile Testing Method for Determining True Stress–Strain Curves for Weldments," *Engineering Fracture Mechanics* 69 (2002): 353–366.

46. J. Baumgartner, A. F. Hobbacher, and R. Rennert, "Fatigue Assessment of Welded Thin Sheets With the Notch Stress Approach – Proposal for Recommendations," *International Journal of Fatigue* 140 (2020): 105844.

47. R. Dantas, M. Gouveia, F. G. A. Silva, et al., "Notch Effect in Very High-Cycle Fatigue Behaviour of a Structural Steel," *International Journal of Fatigue* 177 (2023): 107925.

48. B. Zettl, H. Mayer, C. Ede, and S. Stanzl-Tschegg, "Very High Cycle Fatigue of Normalized Carbon Steels," *International Journal of Fatigue* 28 (2006): 1583–1589.

49. F. Ding, T. Zhao, and Y. Jiang, "A Study of Fatigue Crack Growth With Changing Loading Direction," *Engineering Fracture Mechanics* 74 (2007): 2014–2029.

50. H. Nishikawa, Y. Furuya, T. Kasuya, and M. Enoki, "Microstructurally Small Fatigue Crack Initiation Behavior of Fine and Coarse Grain Simulated Heat-Affected Zone Microstructures in low Carbon Steel," *Materials Science and Engineering A* 832 (2022): 832.

51. H. Nishikawa and Y. Furuya, "Gigacycle Fatigue Fracture of low Strength Carbon Steel, Tested Using a Simulated Heat Affected Zone Microstructure," *ISIJ International* 59 (2019): 1926–1928.

52. F. Liu, Y. Chen, C. He, et al., "Very Long Life Fatigue Failure Mechanism of electron Beam Welded Joint for Titanium Alloy at Elevated Temperature," *International Journal of Fatigue* 152 (2021): 106446.

53. R. A. Lund, "Sheybany S. Fatigue Fracture Appearances," in *Failure Analysis and Prevention* (Materials Park, USA: ASM International, 2002), 627–640.

54. S. Lynch, "Some Fractographic Contributions to Understanding Fatigue Crack Growth," *International Journal of Fatigue* 104 (2017): 12–26.

55. P. Schaumann and S. Steppeler, "Fatigue Tests of Axially Loaded Butt Welds up to Very High Cycles," *Procedia Engineering* 66 (2013): 88–97.

56. R. Rennert, M. Vormwald, and A. Esderts, "FKM-Guideline "Analytical Strength Assessment" – Background and Current Developments," *International Journal of Fatigue* 182 (2024): 108165.

57. R. Zhan, D. Wang, Z. Ren, C. Deng, X. Xu, and H. Liang, "Evolution of Welding Residual Stresses Involving the Cutting Process and Its Effect on Fatigue Performance," *International Journal of Pressure Vessels and Piping* 197 (2022): 104636.

58. H. Liang, Y. Kan, H. Chen, R. Zhan, X. Liu, and D. Wang, "Effect of Cutting Process on the Residual Stress and Fatigue Life of the Welded Joint Treated by Ultrasonic Impact Treatment," *International Journal of Fatigue* 143 (2021): 105998.

59. B. He, H. Deng, M. Jiang, K. Wei, and L. Li, "Effect of Ultrasonic Impact Treatment on the Ultra High Cycle Fatigue Properties of SMA490BW Steel Welded Joints," *International Journal of Advanced Manufacturing Technology* 96 (2018): 1571–1577.

60. Y. Dong and S. C. Guedes, "Stress Distribution and Fatigue Crack Propagation Analyses in Welded Joints," *Fatigue and Fracture of Engineering Materials and Structures* 42 (2019): 69–83.

61. Y. Hong, Y. Hu, and A. Zhao, "Effects of Loading Frequency on Fatigue Behavior of Metallic Materials—A Literature Review," *Fatigue and Fracture of Engineering Materials and Structures* 46 (2023): 3077–3098.

62. C. M. Sonsino, W. Fricke, F. De Bruyne, A. Hoppe, A. Ahmadi, and G. Zhang, "Notch Stress Concepts for the Fatigue Assessment of Welded Joints - Background and Applications," *International Journal of Fatigue* 34 (2012): 2–16.

63. T. Bruder, K. Störzel, J. Baumgartner, and H. Hanselka, "Evaluation of Nominal and Local Stress Based Approaches for the Fatigue Assessment of Seam Welds," *International Journal of Fatigue* 34 (2012): 86–102.